



Simple model for the bottleneck effect in isotropic turbulence based on Kolmogorov's hypotheses

Hao Su (苏豪) 

*State Key Laboratory for Turbulence and Complex Systems, College of Engineering,
Peking University, Beijing 100871, China*

Yue Yang (杨越) *

*State Key Laboratory for Turbulence and Complex Systems, College of Engineering,
Peking University, Beijing 100871, China
and HEDPS-CAPT, Peking University, Beijing 100871, China*

Stephen B. Pope 

*Sibley School of Mechanical and Aerospace Engineering, Cornell University,
Ithaca, New York 14853, USA*



(Received 3 June 2022; accepted 17 January 2023; published 27 January 2023)

We propose a simple model for the bottleneck effect in homogeneous isotropic turbulence as a bump in the compensated energy spectrum, based on Kolmogorov's hypotheses (of 1941 and 1962). The model of the longitudinal structure function consists of two quadratic functions representing large- and small-scale motions. The model parameters are derived from the asymptotic behavior of the structure function. The Kolmogorov and intermittency constants are fitted from direct numerical simulation (DNS) and experimental data. From the model, the height of the spectral bump in the compensated spectrum has a power-law $R_\lambda^{-0.0426}$, and the bump location scaled by the Kolmogorov scale is 0.153, which generally agree with various DNS results at moderate and large Reynolds numbers R_λ . Moreover, we derive that the incorporation of the intermittency exponent into the model leads to the decaying power law of the bump height with R_λ .

DOI: [10.1103/PhysRevFluids.8.014603](https://doi.org/10.1103/PhysRevFluids.8.014603)

I. INTRODUCTION

Kolmogorov [1] proposed several important hypotheses for homogeneous isotropic turbulence (HIT) in 1941 (referred to as K41). They imply that the three-dimensional energy spectrum in HIT can be expressed as

$$E(k) = C\varepsilon^{2/3}k^{-5/3}, \quad (1)$$

in the inertial range, where k denotes the wave number, ε the mean dissipation rate, and C is a constant. Later experiments and simulations found that $E(k)$ presents a small hump as an accumulation of energy, between inertial and dissipation ranges. This “bottleneck effect” was reported by Falkovich and Ryzhenkova [2], and it is then observed in the direct numerical simulation (DNS) [3]. In terms of the compensated spectrum $\Psi(k\eta) = \varepsilon^{-2/3}k^{5/3}E(k)$, where $\eta = (\nu^3/\varepsilon)^{1/4}$ denotes the Kolmogorov length scale with the kinematic viscosity ν , the bottleneck effect manifests itself as a spectral bump in $\Psi(k\eta)$ between the inertial and the dissipation ranges.

*yyg@pku.edu.cn

The bottleneck effect has been quantified in DNS and experiments. Dobler *et al.* [4] pointed out that the bottleneck effect in the three-dimensional energy spectra is more pronounced than in one-dimensional ones. The spectral bump in $E(k)$ can be characterized by its peak location k_b and peak height $\Psi_b \equiv \Psi(k_b\eta)$.

Several DNS [3,5–7] and experimental [8] studies found that Ψ_b decreases with the Reynolds number. Meyers and Meneveau [9] found $\Psi_b \sim \text{Re}^{-\mu/12}$ from DNS data [10], where $\text{Re} = (L/\eta)^{4/3}$ denotes the Reynolds number, with the integral length scale $L = K^3/\varepsilon$, turbulence kinetic-energy K , and the intermittency exponent μ [11]. The Re dependence can be reexpressed as $\Psi_b \sim R_\lambda^{-\mu/6}$ with the widely accepted value of $\mu \approx 0.25$ [12]. Here, $R_\lambda = (15\sigma^4/\nu\varepsilon)^{1/2}$ denotes the Taylor microscale Reynolds number with the root-mean-square velocity fluctuation σ . Donzis and Sreenivasan [5] analyzed a series of DNS results and concluded $\Psi_b \sim R_\lambda^{-0.04}$ and $k_b\eta \approx 0.13$. Küchler *et al.* [8] found the power-law $R_\lambda^{-0.061 \pm 0.007}$ for one-dimensional spectral bumps in recent high-Re experiments.

On the other hand, some DNS [13] and experimental [14] results imply that Ψ_b does not notably decrease with the Reynolds number. These studies [14–17] showed a collapse of one-dimensional spectra in the inertial range, implying the R_λ independence of energy spectra.

The underlying physics of the bottleneck effect has been explained in various ways. Falkovich [18] considered the bottleneck effect as a pileup of energy, in a spectral form of $(k\eta)^{4/3} \ln^{-1}(k\eta)$, from viscous suppression of energy transfer of small-scale modes. Kurien *et al.* [19] also obtained the $k^{-4/3}$ scaling for the bottleneck region from helicity dynamics. Verma and Donzis [20] argued that the pileup of energy is due to insufficient width of the inertial range from energy transfer between different wave-number shells. Frisch *et al.* [21] attributed the bottleneck effect to the incomplete thermalization of high-wave-number modes deduced from hyperviscous Navier-Stokes equations.

There are two approaches for modeling the bottleneck effect. The straightforward one is to find an explicit expression for $E(k)$ in spectral space [9,22,23]. Qian [24] derived an approximate solution for $E(k)$ from two integral equations with the variational method. The result shows the spectral bump in $E(k)$, but it is R_λ independent. Most others are parametrized from DNS results with multiple empirical parameters, and they do not consider the R_λ dependence of the bottleneck effect except in Meyers and Meneveau [9].

The other approach models the structure function $D_n(r)$ in physical space and then calculate $E(k)$. The K41 hypotheses suggest

$$D_n(r) \sim r^{n/3}, \quad (2)$$

in the inertial range. Batchelor [25] proposed an empirical model of the second-order structure function as

$$\frac{D_2(r)}{v_\eta^2} = \frac{1}{15} \frac{\left(\frac{r}{\eta}\right)^2}{\left[1 + (15C_B)^{-3/2} \left(\frac{r}{\eta}\right)^2\right]^{2/3}}, \quad (3)$$

where v_η is the Kolmogorov velocity and C_B is an empirical constant. The quadratic form of this model is supported by theoretical [26] and experimental evidence [27], but Eq. (3) is independent of R_λ .

Lohse and Müller-Groeling [28] argued that besides η used in Batchelor's model [25], another length scale should be incorporated to represent large-scale motion, which can introduce the R_λ dependence. Their model reads

$$D_2(r) = 2\sigma^2 \left(\frac{r^2}{r^2 + r_d^2}\right)^{1-\zeta/2} \left(\frac{r^2}{r^2 + L_0^2}\right)^{\zeta/2}, \quad (4)$$

where r_d and L_0 represent characteristic small and large length scales, respectively, and $\zeta = 2/3$ is a parameter.

Furthermore, the intermittency found in experiments and DNS shows deviations from the power law in Eq. (2). Kolmogorov [11] proposed the refined similarity hypotheses in 1962 (referred to as K62). The introduction of intermittency leads to $D_2(r) \sim r^{2/3+\mu/9}$ in the inertial range, whereas μ is not considered in the model Eq. (3) or (4). The deviation from the K41 theory was also explained by other reasons, such as the finite- R_λ effect [29–32] and the external forcing [33].

Despite the many models for energy spectra and structure functions, there lacks a simple model to predict the bottleneck effect. In the present paper, we propose such a model solely based on K41 and K62 without extra *ad hoc* parameters. Next, the model is developed and validated in Sec. II, the intermittency effect in the model is analyzed in Sec. III, and some conclusions are drawn in Sec. IV.

II. MODELING OF THE BOTTLENECK EFFECT

We develop a simple model based on the second-order longitudinal structure function $D_{LL}(r)$. Note that $D_{LL}(r)$ was used in the K41 hypotheses [1,22] and is related to the second-order structure function as $D_2(r) = 3D_{LL}(r) + r \partial D_{LL}/\partial r$. Following the empirical quadratic forms in Eq. (3) and (4), our model takes the form

$$D_{LL}(r) = C_D \left(\frac{r^2}{r^2 + A\eta^2} \right)^\alpha \left(\frac{r^2}{r^2 + BL^2} \right)^\beta, \quad (5)$$

where model constants C_D , α , β , A , and B are determined by asymptotic results of $D_{LL}(r)$ in the K41 hypotheses, and η and L are characteristic small and large length scales in HIT, respectively.

The K41 hypotheses suggest asymptotic expressions for $D_{LL}(r)$ in high-Re HIT as [22]

$$\begin{aligned} D_{LL}(r) &\rightarrow \frac{\varepsilon}{15\nu} r^2, & r \ll \eta, \\ D_{LL}(r) &\rightarrow C_2(\varepsilon r)^{2/3}, & \eta \ll r \ll L, \\ D_{LL}(r) &\rightarrow 2\sigma^2, & r \gg L, \end{aligned} \quad (6)$$

with the Kolmogorov constant C_2 . Here, the first part is derived from the Taylor expansion of $D_{LL}(r)$ and the hypothesis of local isotropy [1] in the dissipation range with $r \ll \eta$; the second part is from the second similarity hypothesis [1] in the inertial range with $\eta \ll r \ll L$; and the third part is from the definition of $D_{LL}(r)$. Meanwhile, the model in Eq. (5) has limits,

$$\begin{aligned} D_{LL}(r) &\rightarrow C_D \left(\frac{r^2}{A\eta^2} \right)^\alpha \left(\frac{r^2}{BL^2} \right)^\beta, & r \ll \eta, \\ D_{LL}(r) &\rightarrow C_D \left(\frac{r^2}{BL^2} \right)^\beta, & \eta \ll r \ll L, \\ D_{LL}(r) &\rightarrow C_D & r \ll L. \end{aligned} \quad (7)$$

By equating corresponding asymptotic expressions in Eqs. (6) and (7), we determine all constants in Eq. (5) as

$$A = (15C_2)^{3/2}, \quad B = \left(\frac{2\sqrt{6}}{3C_2} \right)^3, \quad C_D = 2\sigma^2, \quad \alpha = \frac{2}{3}, \quad \beta = \frac{1}{3}. \quad (8)$$

The intermittency introduced in the K62 hypotheses [11] suggests

$$D_{LL}(r) \sim r^{2/3+\mu/9}, \quad (9)$$

in the inertial range. Comparing Eq. (9) and the asymptotic expressions $D_{LL}(r) \sim r^{2\beta}$ in the inertial range and $D_{LL}(r) \sim r^{2(\alpha+\beta)} \sim r^2$ in the dissipation range in Eq. (7), we have

$$\alpha = 2/3 - \mu/18 \quad \text{and} \quad \beta = 1/3 + \mu/18. \quad (10)$$

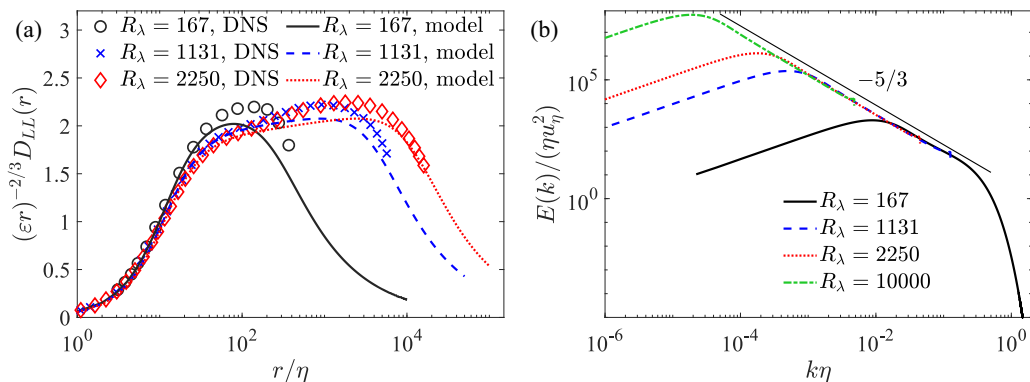


FIG. 1. Normalized (a) longitudinal structure function and (b) energy spectrum at a wide range of R_λ . Lines: model in Eq. (11) with $C_2 = 2.2$ and $\mu = 0.25$; symbols: DNSs [34,35].

Finally, the model of the longitudinal structure function becomes

$$D_{LL}(r) = 2\sigma^2 \left(\frac{r^2}{r^2 + (15C_2)^{3/2}\eta^2} \right)^{2/3-\mu/18} \left(\frac{r^2}{r^2 + [2\sqrt{6}/(3C_2)]^3 L^2} \right)^{1/3+\mu/18}. \quad (11)$$

Note that μ in Eq. (9) can also be introduced in Eq. (6) instead, but we find that the resultant model cannot predict the bottleneck effect well, which is elaborated in Sec. III A.

We assess the model in Eq. (11) by comparing its corresponding $E(k)$ with DNS and the experimental results of HIT. The three-dimensional energy spectrum is calculated from $D_{LL}(r)$ by

$$f(r) = 1 - \frac{1}{2\sigma^2} D_{LL}(r), \quad (12)$$

$$E_{11}(k) = \frac{2\sigma^2}{\pi} \int_0^\infty f(r) \cos(kr) dr, \quad (13)$$

and

$$E(k) = \frac{1}{2} k^3 \frac{d}{dk} \left(\frac{1}{k} \frac{dE_{11}(k)}{dk} \right), \quad (14)$$

where $f(r)$ is the longitudinal correlation function and $E_{11}(k)$ the one-dimensional energy spectrum. In the numerical implementation, Eq. (13) is calculated by the fast Fourier transform, and the derivative in Eq. (14) is calculated by the second-order central difference scheme with an adapted mesh for k . In Eq. (11), we take $C_2 = 2.2$ and $\mu = 0.25$ within widely accepted values [22]. The sensitivity of values of C_2 and μ on modeled $E(k)$ is discussed in Appendix A.

Figure 1 shows profiles of $D_{LL}(r)$ and $E(k)$ at a wide range of R_λ up to 10^4 . In Fig. 1(a), the model in Eq. (11) and DNS data in Ishihara and co-workers [34,35] agree well at small r/η . The introduction of the intermittency component captures the slight growth of the normalized D_{LL} in the inertial range. Otherwise, according to Eq. (6), the profile of the normalized D_{LL} shows a plateau. In Fig. 1(b), the normalized energy spectrum calculated from the model shows that the inertial range broadens with R_λ with a power law close to the $-5/3$ scaling. There exists a small hump between the inertial and dissipation ranges, where $L_{11} = \int_0^\infty f(r) dr$ denotes the longitudinal integral length scale.

Figure 2 compares the modeled $\Psi(k)$ from Eq. (11) with those from the DNS of Donzis and Sreenivasan [5] at a range of R_λ . The modeled $\Psi(k)$ show clear spectral bumps at high wave numbers and their heights decay with R_λ , consistent with the DNS results. Figure 3 compares the heights Ψ_b and locations $k_b\eta$ of spectral bumps between model and various DNS results [3,5,6]. Figure 3(a) shows that Ψ_b from Eq. (11) agrees well with the DNS results. The linear fits $\Psi_b = 2.80R_\lambda^{-0.0426}$

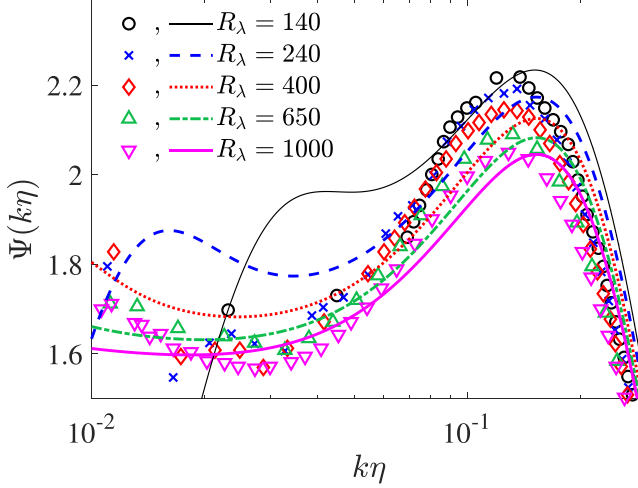


FIG. 2. Comparison of compensated three-dimensional energy spectra with $R_\lambda = 140, 240, 400, 650,$ and 1000 . Symbols: DNS [5]; lines: model in Eq. (11) with $C_2 = 2.2$ and $\mu = 0.25$.

for the model and $\Psi_b = 2.84R_\lambda^{-0.0473}$ for the DNS are close where the power-law exponents are about 20%–30% smaller than that in $R_\lambda^{-0.061 \pm 0.007}$ reported in the experiment [8] with R_λ up to 5000. Figure 3(b) shows that the averaged $k_b\eta = 0.153$ from the model is 20% larger than the averaged $k_b\eta = 0.128$ from the DNS. As discussed in Appendix B, the modeling of $k_b\eta$ can be further improved by introducing an additional parameter in Eq. (11).

III. DEPENDENCE OF THE BOTTLENECK EFFECT ON R_λ

A. Peak height

We derive a scaling of Ψ_b with respect to R_λ from the model in Eq. (11) to show the R_λ dependence in the bottleneck effect. First, $E(k)$ is reexpressed in terms of $D_{LL}(r)$ using Eqs. (12)–(14).

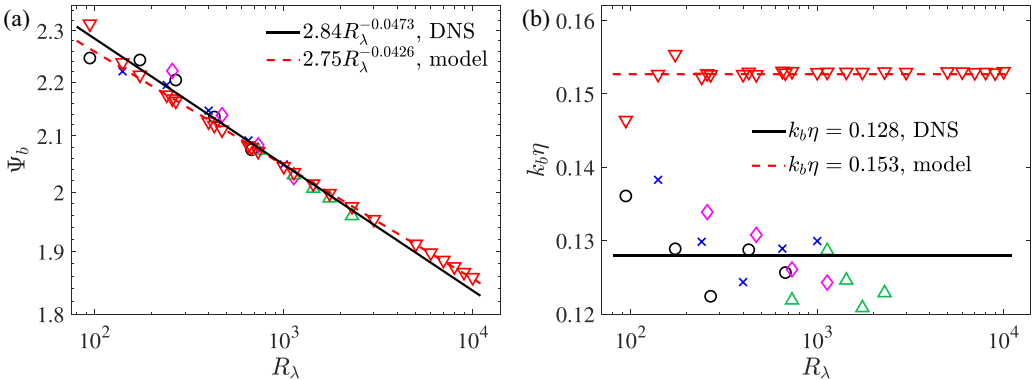


FIG. 3. Comparisons of (a) peak heights and (b) locations of spectral bumps from the model (∇) and DNS data (\circ : Ref. [3]; \times : Ref. [5]; \diamond : Ref. [34]; \triangle : Ref. [6]) with their linear fits or averages (lines). The model results are calculated from Eq. (11) with $C_2 = 2.2$ and $\mu = 0.25$.

Letting $\kappa = k\eta$ and $\xi = kr$, we rewrite Eqs. (13) and (14) as

$$E_{11}(\kappa) = \frac{2\sigma^2\eta}{\pi\kappa} \int_0^\infty f(\xi, \kappa) \cos \xi \, d\xi, \quad (15)$$

and

$$E(\kappa) = \frac{1}{2}\kappa^3 \frac{d}{d\kappa} \left(\frac{1}{\kappa} \frac{dE_{11}}{d\kappa} \right), \quad (16)$$

with

$$f(\xi, \kappa) = 1 - \left(\frac{\xi^2}{\xi^2 + A\kappa^2} \right)^\alpha \left(\frac{\xi^2}{\xi^2 + (20/3)^{-3/2}R_\lambda^3 B\kappa^2} \right)^\beta. \quad (17)$$

In the derivation of Eq. (17), $L/\eta = (20/3)^{-3/4}R_\lambda^{3/2}$ implied from the K41 and Eq. (11) are used.

With Eqs. (15) and (16) and $R_\lambda = (15\sigma^4/\sigma\varepsilon)^{1/2}$, the compensated spectrum is written as

$$\Psi(\kappa) = \frac{R_\lambda}{\sqrt{15\pi}} \kappa^{14/3} \frac{d}{d\kappa} \left(\frac{1}{\kappa} \frac{d}{d\kappa} \int_0^\infty \frac{f(\xi, \kappa)}{\kappa} \cos \xi \, d\xi \right). \quad (18)$$

Assuming $\kappa_b \equiv k_b\eta$ is a constant for simplicity [also see Fig. 3(b)], we consider the relation between $\Psi(\kappa_b)$ and R_λ by estimating the effect of R_λ on the integral in Eq. (18). The integral can be taken as a limit,

$$I(R_\lambda, \kappa) \equiv \lim_{L \rightarrow \infty} \int_0^L \frac{f(\xi, \kappa)}{\kappa} \cos \xi \, d\xi. \quad (19)$$

If the limit exists, the integral can be evaluated by taking a certain series of $L = 2n\pi \rightarrow \infty$ for $\int_0^{2n\pi} \cos \xi / \kappa \, d\xi = 0$. In this way, the constant term in Eq. (17) vanishes in Eq. (19), and then Eq. (19) becomes

$$I(R_\lambda, \kappa) = - \lim_{n \rightarrow \infty} \int_0^{2n\pi} \left(\frac{\xi^2}{\xi^2 + A\kappa^2} \right)^\alpha \left(\frac{\xi^2}{\xi^2 + (20/3)^{-3/2}R_\lambda^3 B\kappa^2} \right)^\beta \cos \xi \, d\xi. \quad (20)$$

Applying the mean value theorem for integrals to Eq. (20), the ratio of integrals for different R_λ , i.e., $R_{\lambda 1}$ and $R_{\lambda 2}$, can be approximated by

$$\frac{I(R_{\lambda 1}, \kappa)}{I(R_{\lambda 2}, \kappa)} \sim \left(\frac{\xi^2 + 15^{-3/2}R_{\lambda 2}^3 B\kappa^2}{\xi^2 + 15^{-3/2}R_{\lambda 1}^3 B\kappa^2} \right)^\beta. \quad (21)$$

Since the integrand in Eq. (19) is a decaying oscillatory function, I is dominated by the integration for small ξ . Thus, Eq. (21) can be approximated by

$$\frac{I(R_{\lambda 1}, \kappa)}{I(R_{\lambda 2}, \kappa)} \sim \left(\frac{R_{\lambda 1}}{R_{\lambda 2}} \right)^{-3\beta}, \quad \xi^2 \ll (20/3)^{-3/2}R_\lambda^3 B\kappa^2. \quad (22)$$

From Eqs. (18) and (22) with Eq. (10), we obtain the scaling,

$$\Psi_b \sim R_\lambda R_\lambda^{-3\beta} = R_\lambda^{-\mu/6} \approx R_\lambda^{-0.042} \quad (23)$$

for $\mu \approx 0.25$.

The power law in Eq. (23) derived from the model of $D_{LL}(r)$ is useful to explain the dependence of Ψ_b on R_λ , although Eqs. (21) and (22) are based on strong approximations. The scaling $R_\lambda^{-\mu/6}$ is consistent with $(k\eta)^{-(5/3+\mu/9)}R_\lambda^{-\mu/6}$ for the normalized spectrum with the intermittency correction [5]. The power-law exponent -0.042 in Eq. (23) agrees with that in Meyers and Meneveau [9] and is close to -0.0426 [see Fig. 3(a)] computed from the modeled $D_{LL}(r)$ in Eq. (11). In particular, the power law implies that the decay of Ψ_b with R_λ is related to the intermittency characterized

by μ in the K62. For $\mu = 0$, Eq. (23) has no R_λ dependence, which is close to a weak power-law $\Psi_b \sim R_\lambda^{-0.007}$ computed from the modeled $D_{LL}(r)$.

Note that if μ is introduced in Eq. (6) as mentioned in Sec. II, the constants in Eq. (8) become $A = [15C_2(15/R_\lambda^2)^{\mu/12}]^{1/\alpha}$ and $B = [2\sqrt{6}/(3C_2)]^{1/\beta}$, and the scaling in Eq. (23) with Eq. (10) becomes

$$\Psi_b \sim R_\lambda R_\lambda^{\mu/6} R_\lambda^{-3\beta} = 1. \quad (24)$$

This result suggests that the peak height has no dependence on R_λ and is inconsistent with the DNS results, so we introduce μ later in Eq. (10).

B. Peak location

The peak location κ_b of the spectral bump satisfies $\Psi'(\kappa_b) = \partial\Psi/\partial\kappa|_{\kappa=\kappa_b} = 0$, and it is written in terms of E_{11} from Eq. (16) as

$$-\frac{4}{3}\kappa_b E'_{11} + \frac{4}{3}\kappa_b^2 E''_{11} + \frac{1}{2}\kappa_b^3 E'''_{11} = 0. \quad (25)$$

As shown in Fig. 2, there are multiple stationary points for $\Psi(\kappa)$, the location for the bottleneck bumps is nearly constant, whereas the locations for other stationary points vary with R_λ . Substituting Eq. (15) into Eq. (25) yields

$$\int_0^\infty \left(f - \kappa_b f' - \frac{1}{6}\kappa_b^2 f'' + \frac{1}{2}\kappa_b^3 f''' \right) \cos \xi \, d\xi = 0, \quad (26)$$

with shorthands f for $f(\xi, \kappa_b)$, f' for $\partial f(\xi, \kappa)/\partial\kappa|_{\kappa=\kappa_b}$, and so on. Taking Eq. (26) as an implicit function $F(\kappa_b, R_\lambda) = 0$, we regard the effect of R_λ on the peak location as $\kappa_b = \kappa_b(R_\lambda)$. Similarly, $f(\xi, \kappa)$ can be written as $f(\xi, \kappa, R_\lambda)$. Taking the derivative of κ_b with R_λ and using Eq. (26), we have

$$\frac{d\kappa_b}{dR_\lambda} = -\frac{\frac{\partial F}{\partial R_\lambda}}{\frac{\partial F}{\partial \kappa_b}} = -\frac{\int_0^\infty (f_R - \kappa_b f'_R - \frac{1}{6}\kappa_b^2 f''_R + \frac{1}{2}\kappa_b^3 f'''_R) \cos \xi \, d\xi}{\int_0^\infty (-\frac{4}{3}\kappa_b f'' + \frac{4}{3}\kappa_b^2 f''' + \frac{1}{2}\kappa_b^3 f'''') \cos \xi \, d\xi}, \quad (27)$$

with the shorthand f'_R for $\partial^2 f(\xi, \kappa, R_\lambda)/\partial\kappa \partial R_\lambda|_{\kappa=\kappa_b}$ and so on.

Theoretical analysis for Eq. (27) appears to be difficult, so instead we seek numerical approximations for Eq. (27) by calculating $\partial F/\partial R_\lambda$ and $\partial F/\partial \kappa_b$ for $R_\lambda = 100$ – $10\,000$ and $\kappa_b = 0.1510$ – 0.1539 , respectively. The numerical results exhibit linear relations,

$$\frac{\partial F}{\partial R_\lambda} \approx 387.6 R_\lambda^{-2.0414} \kappa_b - 59.26 R_\lambda^{-2.0414} \quad \text{and} \quad \frac{\partial F}{\partial \kappa_b} \approx -1012 R_\lambda^{-1.0422} \kappa_b - 218.4 R_\lambda^{-1.0412} \quad (28)$$

for $R_\lambda \geq 500$ where the R_λ dependencies imply power laws of $R_\lambda^{-2-\mu/6}$ and $R_\lambda^{-1-\mu/6}$, respectively. Substituting Eq. (28) into Eq. (27) yields

$$\frac{d\kappa_b}{dR_\lambda} = \frac{1}{R_\lambda} \frac{387.6\kappa_b - 59.26}{1012\kappa_b + 218.4}. \quad (29)$$

The constant κ_b observed in Fig. 3 corresponds to an unstable solution $\kappa_b = 59.26/387.6 \approx 0.153$, consistent with the model results in Fig. 3(b). For smaller κ_b , Eq. (29) has $d\kappa_b/dR_\lambda < 0$, corresponding to the other stationary points of $\Psi(k\eta)$.

IV. CONCLUSIONS

We propose a simple model for the bottleneck effect in the energy spectrum of HIT solely based on the K41 and K62 hypotheses. The model of the longitudinal structure function $D_{LL}(r)$ in Eq. (11) consists of two quadratic functions of r representing large and small length scales. The model parameters are derived from the asymptotic behavior of $D_{LL}(r)$. The Kolmogorov and intermittency constants (i.e., C_2 and μ in the K41 and K62 hypotheses) are fitted from DNS and experimental data.

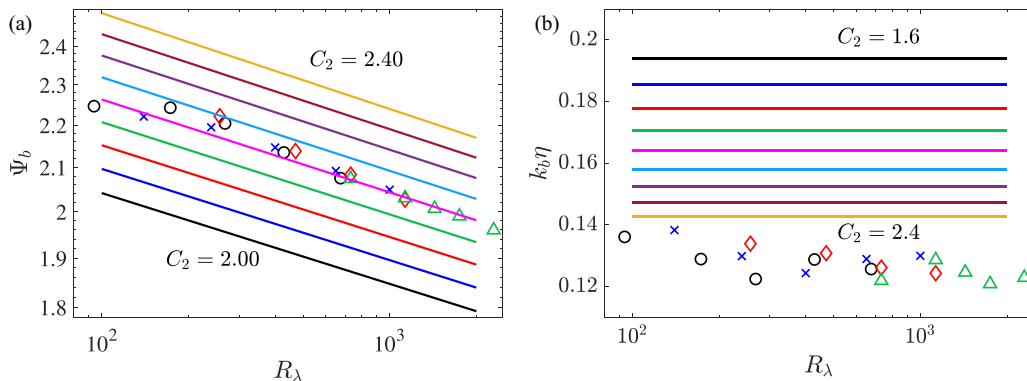


FIG. 4. Effects of the variation in C_2 on modeling the (a) height and (b) location of the spectral bumps of $\Psi(k\eta)$ at a range of R_λ with $\mu = 0.25$. Lines in (a): linear fits of modeling results with $C_2 = 2.0, 2.05, \dots, 2.40$, from bottom to top; lines in (b): averages of modeling results with $C_2 = 1.6, 1.7, \dots, 2.4$, from top to bottom; symbols: DNS results (\circ : Ref. [3], \times : Ref. [5], \diamond : Ref. [34], and \triangle : Ref. [6]).

The modeling of the bottleneck effect by Eq. (11) with $C_2 = 2.2$ and $\mu = 0.25$ is validated using DNS and experimental data at moderate and high Reynolds numbers. The height of the spectral bump calculated from the model has the power-law $\Psi_b = 2.8R_\lambda^{-0.0426}$, which has a good agreement with $\Psi_b = 2.84R_\lambda^{-0.0473}$ in the DNS [3,5,6]. The location of the spectral bump from the model is $k_b\eta = 0.153$ is 20% larger than $k_b\eta = 0.128$ in the DNS, and the further model improvement is discussed in Appendix B. Note that to show the predictability, all parameters in the model are fixed for various HIT cases with a wide range of R_λ . The sensitivity of C_2 and μ on modeling results is discussed in Appendix A, and the present model and existing ones are compared in Appendix C.

To demonstrate the R_λ dependence in the bottleneck effect, we theoretically derive that the incorporation of the intermittency exponent into the model leads to the power-law $\Psi_b \sim R_\lambda^{-\mu/6} \approx R_\lambda^{-0.042}$, consistent with modeling and DNS results. In addition, the model implies that $k_b\eta$ approaches to a constant at large R_λ .

ACKNOWLEDGMENTS

This work has been supported, in part, by the National Natural Science Foundation of China (Grants No. 11988102 and No. 11925201), the National Key R&D Program of China (Grant No. 2020YFE0204200) and the Xplore Prize.

APPENDIX A: SENSITIVITY OF EMPIRICAL CONSTANTS IN THE BOTTLENECK EFFECT

There are two empirical constants, the Kolmogorov constant C_2 and the intermittency exponent μ , in the K41 and K62 hypotheses, respectively. Scattered values of C_2 and μ were reported within moderate ranges in the literature due to uncertainties in determining them in high-Re experiments [8] or DNS [5,6]. Hence, we examine the sensitivity of them on Ψ_b and k_b computed from the modeled $D_{LL}(r)$ in Eq. (11).

First, we vary C_2 from 1.6 to 2.4 based on its values reported in the literature [5,6,13]. The resultant heights and locations of the bottleneck are shown in Fig. 4. Figure 4(a) shows that Ψ_b increases with C_2 because the total energy in the inertial range grows linearly with C_2 implied by Eq. (1) with the relation $C = 55C_2/[27\Gamma(1/3)]$ [27]. Moreover, the power-law exponent γ in $\Psi_b \sim R_\lambda^\gamma$ remains almost constant as the theoretical result in Eq. (23). Figure 4(b) shows that $k_b\eta$ decreases with increasing C_2 . The bottleneck effect can be considered as an accumulation of energy between inertial and dissipation ranges when the energy transfers from larger to smaller length

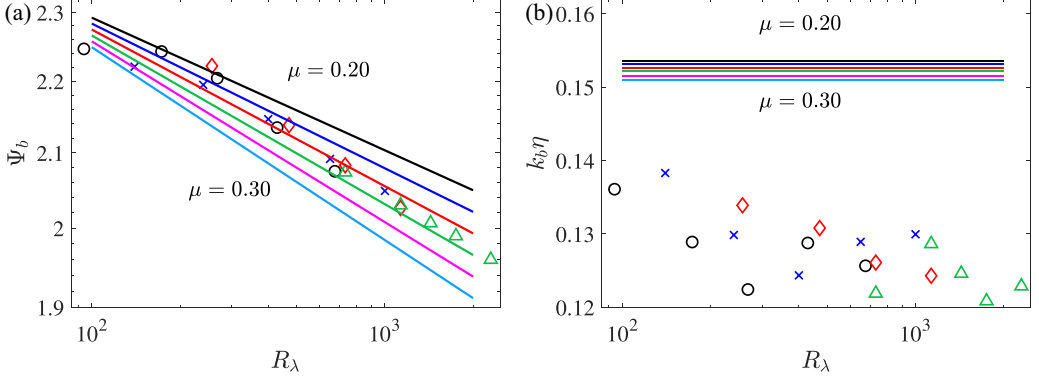


FIG. 5. Effects of the variation in μ on modeling the (a) height and (b) location of the spectral bumps of $\Psi(k\eta)$ at a range of R_λ with $C_2 = 2.2$. Lines in (a): linear fits of modeling results with $\mu = 0.20, 0.22, \dots, 0.30$, from top to bottom; lines in (b): averages of modeling results with $\mu = 0.20, 0.22, \dots, 0.30$, from top to bottom; symbols: DNS results (\circ : Ref. [3], \times : Ref. [5], \diamond : Ref. [34], and \triangle : Ref. [6]).

scales. Increasing C_2 causes a uniform rise of $E(k)$ in the inertial range, and then the pileup of energy could occur earlier in the energy transfer, i.e., $k_b\eta$ becomes smaller.

Second, we vary μ from 0.2 to 0.3 [12] to show the intermittency effect on Ψ_b and $k_b\eta$ in Fig. 5. In Fig. 5(a), Ψ_b and the power-law exponent decrease with increasing μ . From the scaling $E(k) \sim k^{-(5/3+\mu/9)}$ with the intermittency correction [5], the growth of μ appears to suppress the energy at large k . In Fig. 5(b), $k_b\eta$ only slightly decreases with μ , indicating that the intermittency has a minor influence on the location of the spectral bump.

Based on the sensitive study, we choose $C_2 = 2.2$ and $\mu = 0.25$ in the model of $D_{LL}(r)$ in Eq. (11) for the overall best fit of DNS data.

APPENDIX B: IMPROVEMENT ON MODELING THE BOTTLENECK LOCATION

To further improve the modeling results in Figs. 2 and 3, we introduce two parameters p and q to Eqs. (5) and (11) as

$$D_{LL}(r) = C_D \left(\frac{r^p}{r^p + A^{p/2}\eta^p} \right)^{2(\alpha-\mu/18)/p} \left(\frac{r^q}{r^q + B^{q/2}L^q} \right)^{2(\beta+\mu/18)/q}. \quad (\text{B1})$$

The asymptotic expressions of Eq. (B1) with $\mu = 0$ are the same as Eq. (6), so the values of $C_D, A, B, \alpha,$ and β in Eq. (8) remain in Eq. (B1). For the compensated spectrum calculated from Eq. (B1), we find that Ψ_b and k_b grow with increasing p , whereas $\Psi(k\eta)$ at small k is almost unchanged. Similarly, $\Psi(k\eta)$ only grows at small k with q .

Based on the sensitivity analysis in Appendix A, we vary only p and C_2 and keep $q = 2$ and $\mu = 0.25$ in Eq. (B1), and obtain $p = 1.8$ and $C_2 = 2.3$ for the best fit of Ψ_b and k_b with the DNS results. In Fig. 6, the spectral bumps calculated from the model of Eq. (B1) show a better agreement with the DNS result [5] than the model of Eq. (11) at $k\eta \geq 0.1$, whereas, $\Psi(k\eta)$ from the model of Eq. (B1) is overestimated at $k\eta < 0.1$.

In Fig. 7(a), the estimations of Ψ_b from Eqs. (11) and (B1) are very close, and they agree well with the DNS results [3,5,6]. In Fig. 7(b), the model of (B1) performs better than Eq. (11), showing excellent agreement with the DNS results at large R_λ . Moreover, the model of Eq. (B1) has the same scaling of $\Psi_b = R_\lambda^{-\mu/6}$ in Eq. (23), and its $d\kappa_b/dR_\lambda$ in Eq. (27) has an unstable solution $\kappa_b \approx 0.1271$.

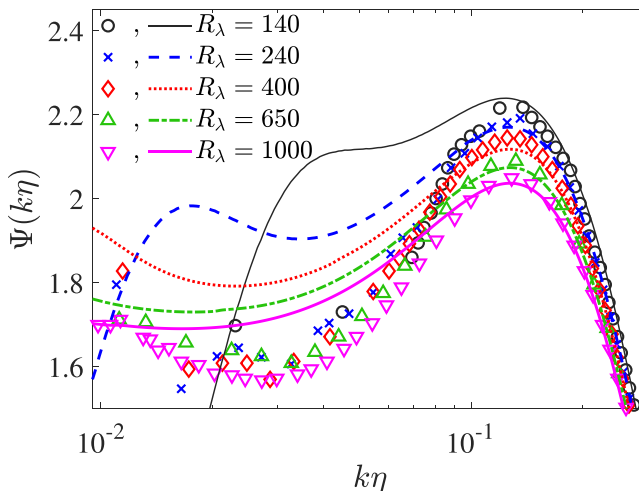


FIG. 6. Comparison of compensated three-dimensional energy spectra with $R_\lambda = 140, 240, 400, 650,$ and 1000 . Symbols: DNS [5]; lines: model in Eq. (B1) with $p = 1.8, q = 2, C_2 = 2.3,$ and $\mu = 0.25$.

APPENDIX C: COMPARISON OF MODELS FOR THE BOTTLENECK EFFECT

We compare the present model with typical existing ones on the prediction of the bottleneck effect. Starting from Eq. (1) in the K41, it is straightforward to model the bump of $E(k)$ in spectral space. Pope [22] introduced a simple model spectrum,

$$E(k) = C\varepsilon^{2/3}k^{-5/3}f_L(kL)f_\eta(k\eta), \quad (\text{C1})$$

where f_L and f_η are nondimensional functions for energy-containing and dissipation ranges, respectively. Since f_η in Eq. (C1) is in the form of exponential decay, this simple model does not show the spectral bump. Lamorgese *et al.* [23] developed an empirical model of f_η to represent the bump using a complicated function with several model parameters fitted from the DNS. However, we find that, in this model, the major R_λ dependency comes from f_L , so the spectral bump is almost independent of R_λ at moderate and large R_λ . Meyers and Meneveau [9] introduce the intermittency to Eq. (1), and parametrized the bottleneck in the functional form of $E(k)$, containing five model

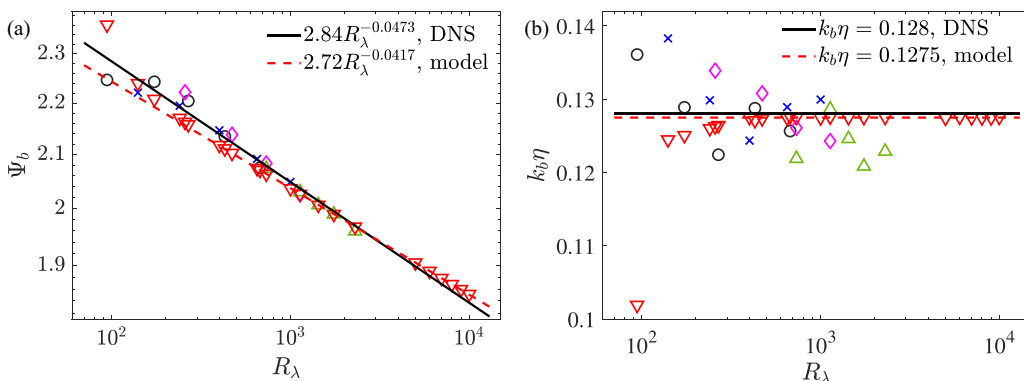


FIG. 7. Comparisons of (a) peak heights and (b) locations of spectral bumps from the model (∇) and DNS data (\circ : Ref. [3]; \times : Ref. [5]; \diamond : Ref. [34]; \triangle : Ref. [6]) with their linear fits or averages (lines). The model results are calculated from Eq. (B1) with $p = 1.8, q = 2, C_2 = 2.3, \mu = 0.25,$ and Eq. (8).

parameters computed from five constraints and DNS data. We find that the height and location of the bottleneck from this model agree well with those in DNS.

For modeling in physical space, Eqs. (3) and (4) without the intermittency exponent show the independence and weak dependence of R_λ of the bottleneck effect, respectively. Antonia *et al.* [36] proposed an empirical model for the second-order structure function without the intermittency exponent. This model has two parameters that can be adjusted in different flows and achieves good agreement with experimental results in both small and large scales. However, we find that Ψ_b computed from this model is almost independent on R_λ . Gravanis and Akylas [37] proposed a generalized Batchelor model [25]. The expansion of $f(r)$ contains a series of quadratic functions of r , and each term represents a length scale and has two empirical parameters, which can be fitted from the data. Their model with two scales can capture the bottleneck in DNS well, but the empirical parameters are not universal for different R_λ .

Thus, compared to the simple model in Eq. (11), some of the existing models can also achieve good agreement on the bottleneck effect with the DNS data, but they contain much more functional forms and empirical parameters fitted from the DNS, and they show no explicit dependence of the bottleneck effect on R_λ as in Eq. (23).

-
- [1] A. N. Kolmogorov, The local structure of turbulence in incompressible viscous fluid for very large Reynolds numbers, *Proc. R. Soc. London, Ser. A* **434**, 9 (1991).
 - [2] G. Falkovich and I. Ryzhenkova, Influence of dissipation on Kolmogorov spectra of wave turbulence, *Sov. Phys. JETP* **71**, 1085 (1990).
 - [3] T. Ishihara, Y. Kaneda, M. Yokokawa, K. Itakura, and A. Uno, Energy spectrum in the near dissipation range of high resolution direct numerical simulation of turbulence, *J. Phys. Soc. Jpn.* **74**, 1464 (2005).
 - [4] W. Dobler, N. E. L. Haugen, T. A. Yousef, and A. Brandenburg, Bottleneck effect in three-dimensional turbulence simulations, *Phys. Rev. E* **68**, 026304 (2003).
 - [5] D. A. Donzis and K. R. Sreenivasan, The bottleneck effect and the Kolmogorov constant in isotropic turbulence, *J. Fluid Mech.* **657**, 171 (2010).
 - [6] T. Ishihara, K. Morishita, M. Yokokawa, A. Uno, and Y. Kaneda, Energy spectrum in high-resolution direct numerical simulations of turbulence, *Phys. Rev. Fluids* **1**, 082403(R) (2016).
 - [7] S. Khurshid, D. A. Donzis, and K. R. Sreenivasan, Energy spectrum in the dissipation range, *Phys. Rev. Fluids* **3**, 082601(R) (2018).
 - [8] C. Küchler, G. Bewley, and E. Bodenschatz, Experimental study of the bottleneck in fully developed turbulence, *J. Stat. Phys.* **175**, 617 (2019).
 - [9] J. Meyers and C. Meneveau, A functional form for the energy spectrum parametrizing bottleneck and intermittency effects, *Phys. Fluids* **20**, 065109 (2008).
 - [10] U. Kaneda, T. Ishihara, M. Yokokawa, K. Itakura, and A. Uno, Energy dissipation rate and energy spectrum in high resolution direct numerical simulations of turbulence in a periodic box, *Phys. Fluids* **15**, L21 (2003).
 - [11] A. N. Kolmogorov, A refinement of previous hypotheses concerning the local structure of turbulence in a viscous incompressible fluid at high Reynolds number, *J. Fluid Mech.* **13**, 82 (1962).
 - [12] K. R. Sreenivasan and P. Kailasnath, An update on the intermittency exponent in turbulence, *Phys. Fluids A* **5**, 512 (1993).
 - [13] P. K. Yeung and Y. Zhou, Universality of the Kolmogorov constant in numerical simulations of turbulence, *Phys. Rev. E* **56**, 1746 (1997).
 - [14] S. G. Saddoughi and S. V. Veeravalli, Local isotropy in turbulent boundary layers at high Reynolds number, *J. Fluid Mech.* **268**, 333 (1994).
 - [15] J. V. Larssen and W. J. Devenport, On the generation of large-scale homogeneous turbulence, *Exp. Fluids* **50**, 1207 (2011).

- [16] R. A. Antonia, L. Djenidi, and L. Danaila, Collapse of the turbulent dissipative range on Kolmogorov scales, *Phys. Fluids* **26**, 045105 (2014).
- [17] M. Vallikivi, B. Ganapathisubramani, and A. J. Smits, Spectral scaling in boundary layers and pipes at very high Reynolds numbers, *J. Fluid Mech.* **771**, 303 (2015).
- [18] G. Falkovich, Bottleneck phenomenon in developed turbulence, *Phys. Fluids* **6**, 1411 (1994).
- [19] S. Kurien, M. A. Taylor, and T. Matsumoto, Cascade time scales for energy and helicity in homogeneous isotropic turbulence, *Phys. Rev. E* **69**, 066313 (2004).
- [20] M. K. Verma and D. Donzis, Energy transfer and bottleneck effect in turbulence, *J. Phys. A: Math. Theor.* **40**, 4401 (2007).
- [21] U. Frisch, S. Kurien, R. Pandit, W. Pauls, S. S. Ray, A. Wirth, and J. Z. Zhu, Hyperviscosity, Galerkin Truncation, and Bottlenecks in Turbulence, *Phys. Rev. Lett.* **101**, 144501 (2008).
- [22] S. B. Pope, *Turbulent Flows* (Cambridge University Press, Cambridge, UK, 2000).
- [23] A. G. Lamorgese, D. A. Caughey, and S. B. Pope, Direct numerical simulation of homogeneous turbulence with hyperviscosity, *Phys. Fluids* **17**, 015106 (2005).
- [24] J. Qian, Universal equilibrium range of turbulence, *Phys. Fluids* **27**, 2229 (1984).
- [25] G. K. Batchelor, Pressure fluctuations in isotropic turbulence, *Math. Proc. Cambridge Philos. Soc.* **47**, 359 (1951).
- [26] L. Sirovich, L. Smith, and V. Yakhot, Energy Spectrum of Homogeneous and Isotropic Turbulence in Far Dissipation Range, *Phys. Rev. Lett.* **72**, 344 (1994).
- [27] A. S. Monin and A. M. Yaglom, *Statistical Fluid Mechanics: Mechanics of Turbulence* (The MIT Press, Cambridge, MA, 1975).
- [28] D. Lohse and A. Müller-Groeling, Bottleneck Effects in Turbulence: Scaling Phenomena in r Versus p Space, *Phys. Rev. Lett.* **74**, 1747 (1995).
- [29] J. Qian, Closure Approach to High-Order Structure Functions of Turbulence, *Phys. Rev. Lett.* **84**, 646 (2000).
- [30] T. S. Lundgren, Kolmogorov two-thirds law by matched asymptotic expansion, *Phys. Fluids* **14**, 638 (2002).
- [31] J. Tchoufag, P. Sagaut, and C. Cambon, Spectral approach to finite Reynolds number effects on Kolmogorov's $4/5$ law in isotropic turbulence, *Phys. Fluids* **24**, 015107 (2012).
- [32] S. L. Tang, R. A. Antonia, L. Djenidi, L. Danaila, and Y. Zhou, Finite Reynolds number effect on the scaling range behaviour of turbulent longitudinal velocity structure functions, *J. Fluid Mech.* **820**, 341 (2017).
- [33] L. Djenidi and R. A. Antonia, Kármán–howarth solutions of homogeneous isotropic turbulence, *J. Fluid Mech.* **932**, A30 (2022).
- [34] T. Ishihara, T. Gotoh, and Y. Kaneda, Study of high-Reynolds number isotropic turbulence by direct numerical simulation, *Annu. Rev. Fluid Mech.* **41**, 165 (2009).
- [35] T. Ishihara, Y. Kaneda, K. Morishita, M. Yokokawa, and A. Uno, Second-order velocity structure functions in direct numerical simulations of turbulence with $R\lambda$ up to 2250, *Phys. Rev. Fluids* **5**, 104608 (2020).
- [36] R. A. Antonia, S. L. Tang, L. Djenidi, and Y. Zhou, Finite Reynolds number effect and the $4/5$ law, *Phys. Rev. Fluids* **4**, 084602 (2019).
- [37] E. Gravanis and E. Akylas, Generalized Batchelor functions of isotropic turbulence, *Phys. Fluids* **27**, 015101 (2015).